Transient dynamics and structure of optimal excitations in thermocapillary spreading: Precursor film model

Jeffrey M. Davis[a)]
Department of Chemical Engineering, University of Massachusetts, Amherst, Masachusetts 01003

Dawn E. Kataoka
Sandia National Laboratories, Livermore, California 94551

Sandra M. Troian[b)]
Department of Applied Physics, California Institute of Technology, 1200 East California Boulevard, M/C 128-95, Pasadena, California 91125

(Received 15 February 2006; accepted 7 August 2006; published online 5 September 2006)

Linearized modal stability theory has shown that the thermocapillary spreading of a liquid film on a homogeneous, completely wetting surface can produce a rivulet instability at the advancing front due to formation of a capillary ridge. Mechanisms that drain fluid from the ridge can stabilize the flow against rivulet formation. Numerical predictions from this analysis for the film speed, shape, and most unstable wavelength agree remarkably well with experimental measurements even though the linearized disturbance operator is non-normal, which allows transient growth of perturbations. Our previous studies using a more generalized nonmodal stability analysis for contact lines models describing partially wetting liquids (i.e., either boundary slip or van der Waals interactions) have shown that the transient amplification is not sufficient to affect the predictions of eigenvalue analysis. In this work we complete examination of the various contact line models by studying the influence of an infinite and flat precursor film, which is the most commonly employed contact line model for completely wetting films. The maximum amplification of arbitrary disturbances and the optimal initial excitations that elicit the maximum growth over a specified time, which quantify the sensitivity of the film to perturbations of different structure, are presented. While the modal results for the three different contact line models are essentially indistinguishable, the transient dynamics and maximum possible amplification differ, which suggests different transient dynamics for completely and partially wetting films. These differences are explained by the structure of the computed optimal excitations, which provides further basis for understanding the agreement between experiment and predictions of conventional modal analysis. © *2006 American Institute of Physics*. [DOI: 10.1063/1.2345372]

I. INTRODUCTION

Efforts to manipulate fluid flow with microelectromechanical devices (MEMS) have directed attention to the dominant role of surface forces in controlling the movement of thin liquid films.[1–3] Because of their small size, these micronic devices contain large surface to volume ratios, thereby producing a liquid environment that is highly susceptible to stresses at the air-liquid or liquid-solid interface.[4] For simple fluids, large surface stresses can arise from thermal or composition variations at the air-liquid surface. In particular, the behavior of thin Newtonian liquid films driven to spread by thermocapillary forcing has been studied during the past few years.[5–20] A thin wetting film in contact with a solid surface bearing a thermal gradient experiences a surface shear stress that forces the liquid to spread from warmer to cooler regions. Complete surface coverage may be compromised by the nucleation of holes or dry spots in the spreading film or by a rivulet instability at the leading edge that can leave strips of the surface dry and exposed. Careful manipulation of the forces responsible for spreading, however, will suppress the rivulet instability. Application of a counterflow[7] can prevent rivulet formation at the advancing front of spreading films and encourage complete surface coverage.[21] Furthermore, dynamic adjustment of the local temperature gradient based on continuous optical feedback has been used to inhibit the rivulet instability in otherwise unstable flows.[22] Thermocapillary driven spreading provides a good prototype for understanding the strong influence surface stresses can exert and how these stresses affect the dynamics and stability of thin liquid films.

Experimental studies of thermocapillary driven films in both vertical[23–26] and horizontal[27] orientations have shown that larger thermal gradients produce thinner spreading films that develop a capillary ridge at the spreading front. As the spreading proceeds, this ridge is observed to separate into numerous equally spaced rivulets or "fingers." A typical example of the shape transformation leading to the fingering instability is shown in Fig. 1. By contrast, smaller applied gradients produce thicker films with no ridge formation or subsequent fingering at the spreading front.[21] The dynamics of the forced spreading process and the conditions leading to

[a)]Electronic mail: jmdavis@ecs.umass.edu
[b)]Electronic mail: stroian@princeton.edu

 © 2006 American Institute of Physics

Downloaded 28 Oct 2008 to 131.215.237.157. Redistribution subject to AIP license or copyright; see http://pof.aip.org/pof/copyright.jsp

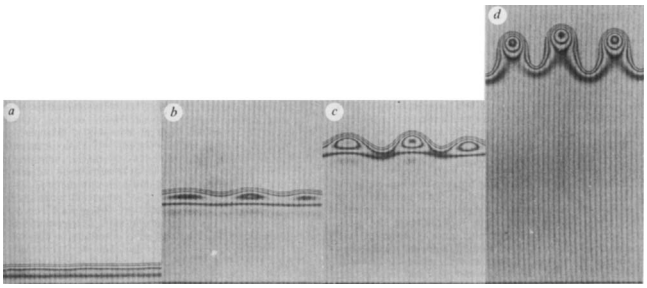

FIG. 1. Optical micrograph reproduced from Fig. 2 of Ref. 23 showing the evolution of a fingering instability at the advancing front of a silicon oil film (μ=20 mPa s) on a silicon wafer. The applied thermal stress was τ =0.18 Pa. The instability wavelength, which remains constant in time, was approximately 500 μm. The time corresponding to each image is (a) 1.5 min, (b) 6.5 min, (c) 10 min, and (d) 17 min.

unstable flow seem well captured by linear modal stability analysis for both large and small thermal gradients. Numerical solutions have successfully described the speed and shape of the spreading film before rivulet formation, as well as the range of stability, the perturbed shape, and the wavelength selection for unstable flow.[6,7] This analysis has also confirmed that the additional presence of significant gravitational drainage in thicker, vertically climbing films drains fluid from the front to eliminate the ridge, thereby stabilizing the spreading process against frontal breakup. These studies suggest that any mechanism that can effectively draw liquid out from under the capillary ridge will prevent rivulet formation and produce complete surface coverage, at least for the case of completely wetting fluids.

Rivulet formation in thermocapillary driven films is but one manifestation of a generic fingering instability that occurs in wetting films driven to spread across a dry surface.[28] The same instability has been observed in films driven to spread by gravity,[29–31] centrifugation,[32–34] or a blowing gas stream.[32] For the most part, agreement with the linearized modal description has been quite good. As first observed for gravitationally driven flows,[35,36] however, the linearized operator governing the evolution of disturbances is non-normal in form. Because of this non-normality, the usual eigenanalysis identifying the most unstable wavelength predicts only the asymptotic behavior of the linearized dynamical system as $t \to \infty$. In general, the eigenanalysis may not predict the spreading dynamics at finite times during which large transient growth may occur.

It has been suggested in the literature that certain nonmodal systems can produce tremendous amplification of initially small disturbances at early or intermediate times that may eclipse the asymptotic behavior and induce nonlinear effects.[35,37–41] The transient behavior of disturbances to thermally driven films has recently been examined for two different models used to relieve the stress singularity at the moving contact line: a structured precursor film whose shape is governed by van der Waals interactions[8] and slip at the liquid-solid interface.[9,10,14] The ability to specify the slip coefficient and contact angle independently allows this latter model to account for partially wetting liquids. These investigations indicate that transient growth is relatively unimportant in thermally driven films but that the magnitude and duration of this growth can depend strongly on the contact line model employed. In this present work, this transient analysis is extended to models of thermocapillary spreading based on a flat precursor film, which is the most widely used model for spreading films with various driving forces.[42,43]

This study is an extension of our recent studies[8–10,44] of the transient dynamics and optimal excitations for other contact line models. The flat precursor film model used in this investigation is based on the presence of a precursor film of uniform thickness beyond the nominal contact line[42,45] and is used to model completely wetting fluids. This precursor film can be coated onto a substrate or can develop as the result of evaporation and condensation processes or surface diffusion at the advancing front of the spreading film. Such a precursor film has been observed in slowly advancing, wetting films driven by thermal gradients,[21] making this boundary condition a relevant choice for this analysis.

Emphasis is placed on determining the structure of perturbations that experience the most amplification, which differs significantly for each contact line model. Both thin films with capillary ridges and thicker films, in which gravitational drainage suppresses ridge formation, are considered. The results reveal the evolution of an initial disturbance toward the eigenfunction described by modal analysis, what type of initial conditions most effectively excite the mean flow to produce rivulets at the spreading front, and on what time scales the transient behavior crosses over to the asymptotic solutions.

While there are many recent theoretical and computational studies of thin liquid films driven to spread by thermocapillary stresses or gravity,[6–16,46–52] this is the first investigation to compute explicitly the optimal excitations for thermocapillary spreading with the common precursor film model. When compared to results for the slip model[10] for partially wetting fluids, the results provide insights into the influence of wetting properties on the amplification of disturbances and reveal important differences between the models, as discussed in Secs. III and V below. Furthermore, as detailed in Sec. II, the gravitational counterflow that drains the capillary ridge for thicker climbing films can significantly alter the dynamics. The influence of this (convective) term on the dynamics[11,12,53] is much richer than that of the stabilizing (diffusive) hydrostatic term that can become significant for films falling along slightly inclined planes.[35,44] The transient behavior and optimal excitations for this case are found to differ from the more extensively investigated regime of thinner films in which drainage is negligible.

II. GOVERNING EQUATIONS

The equations governing the behavior of a thermally driven film in either vertical or horizontal geometry have been derived previously.[6,7] For brevity, only the relevant equations for a vertically climbing film in the presence and absence of gravitational drainage are presented. The formulation is easily extended to any angle of inclination with respect to the horizontal. The reader is referred to earlier work[6,7] for details of the complete derivation including jus-

Downloaded 28 Oct 2008 to 131.215.237.157. Redistribution subject to AIP license or copyright; see http://pof.aip.org/pof/copyright.jsp

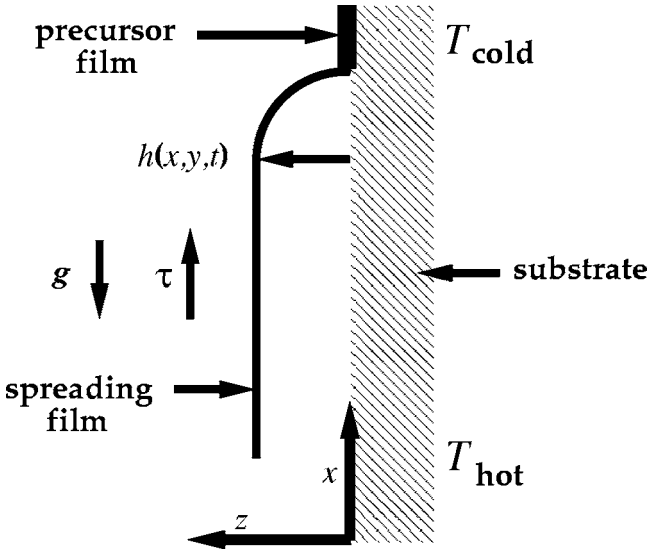

FIG. 2. Schematic diagram of a liquid film climbing a vertical substrate under the action of a constant shear stress, τ. Thicker climbing films are also subject to gravitational drainage represented by the opposing acceleration, g.

tification of the relevant scalings and boundary conditions used.

Consider the thermocapillary driven flow of a completely wetting, Newtonian liquid film of density ρ and viscosity μ. The liquid is supplied from a source at constant flux. Immersed in the liquid reservoir is a vertical substrate bearing a constant thermal gradient whose warmer side is located at the lower end of the substrate. For sufficiently thin films, the Biot number is small, and the applied vertical temperature gradient at the liquid-solid surface is equal to that at the air-liquid interface. Application of a linear thermal gradient produces a constant shear stress, τ, that drives the liquid film up the plate. Gravitational drainage can lessen the upwardly directed flux. Within the lubrication approximation and near the front of the spreading film, there exists an inner region of the flow where capillary forces are significant since the interface must bend to meet the solid surface. Here, the evolution of the local film thickness, $\bar{h}(x,y,t)$, is governed by[6–8,54]

$$\frac{\partial \bar{h}}{\partial \bar{t}} + \frac{\partial}{\partial x}\left(\frac{\tau \bar{h}^2}{2\mu} - \frac{\rho g \bar{h}^3}{3\mu}\right) + \nabla \cdot \left[\frac{\bar{h}^3}{3\mu}\nabla(\gamma \nabla^2 \bar{h})\right] = 0, \qquad (1)$$

where g denotes gravitational acceleration and γ is the surface tension. Within this small inner region, the viscosity μ and surface tension γ in the capillary force term are assumed constant.[6] The coordinate system is defined such that x represents the vertical direction of flow, y the spanwise direction, and z the direction perpendicular to the substrate, as shown in Fig. 2. The gravitational term in Eq. (1) is ignored for film thicknesses $h_c \ll \tau/\rho g$ but retained for $h_c \sim \tau/\rho g$. Both regimes are considered when analyzing the spreading dynamics below.

Equation (1) is converted to dimensionless form through introduction of the transformations $(\chi,\zeta)=l^{-1}(-x,y)$, $h=\bar{h}/h_c$, and $t=\bar{t}/(l/u_c)$. The dynamic capillary length, $l=h_c(3\,\mathrm{Ca})^{-1/3}$, represents the characteristic scale over which capillary forces compete with the thermocapillary force and viscous drag.[28,29] The capillary number is defined by $\mathrm{Ca}=\mu u_c/\gamma$, where $u_c=h_c\tau/2\mu$ or $u_c=h_c\tau/2\mu-\rho g h_c^2/3\mu$ depending on whether or not gravitational drainage presents a counterflow. The film thickness, h_c, denotes the characteristic thickness far from the leading edge (the "outer region") where capillary forces are insignificant. For very thin films in which drainage is negligible, the value of h_c is set by the experimental conditions at the upstream end which determine the film thickness emerging from the meniscus region at the liquid source.[25,26,55] When drainage is significant, the value is set by the ratio $\alpha\tau/\rho g$, where α is a proportionality constant describing the relative strength between drainage and Marangoni forces. For the case of competing thermocapillary and gravitational forces, there exists a rich structure of compressive traveling waves (Lax shocks), "undercompressive" traveling waves, and multiple traveling waves depending on the relative strength of the forces and the precursor film thickness.[11,12,53] Attention here is restricted to the monotonically decreasing fronts (corresponding to undercompressive traveling wave solutions) that arise for comparable thermocapillary and gravitational forces (α near unity), which were previously found to be in good agreement with experimental data.[7] In keeping with prior calculations, the sign of ξ has been reversed so that this coordinate increases in the direction of the liquid reservoir. The dimensionless form of Eq. (1) is given by

$$h_t - [h^2 - h^3(\nabla^2 h)_\chi]_\chi + [h^3(\nabla^2 h)_\zeta]_\zeta = 0 \quad \text{for } h_c \ll \tau/\rho g \qquad (2)$$

and

$$h_t - \left[\frac{3}{3-2\alpha}h^2 - \frac{2\alpha}{3-2\alpha}h^3 - h^3(\nabla^2 h)_\chi\right]_\chi + [h^3(\nabla^2 h)_\zeta]_\zeta = 0 \quad \text{for } h_c = \alpha\tau/\rho g, \qquad (3)$$

where $\nabla^2=\partial_{\chi\chi}+\partial_{\zeta\zeta}$ and subscripts denote partial differentiation with respect to χ,ζ or t. Attention is restricted to $\alpha<3/2$, which corresponds to a net upward flux of liquid.[7]

A. Steady state solutions

The base flow solutions to Eqs. (2) or (3), which describe one-dimensional flow in the streamwise direction, $\hat{\chi}$, are solved subject to the boundary conditions $h\to 1$ and $h_{\chi\chi\chi}\to 0$ as $\chi\to+\infty$ and $h\to b$ and $h_{\chi\chi\chi}\to 0$ as $\chi\to-\infty$. The condition $h\to b$ as $\xi\to-\infty$, with $b\ll 1$, reflects the presence of an ultrathin wetting film ahead of the nominal contact line. This prewetting film serves to alleviate the stress singularity arising from the no slip condition at a moving contact line,[42,43,45,56] as previously implemented in a number of spreading problems.[6,7,28,56–58] Although it has not been established experimentally that this precursor film exists in rapid coating flows or flows using partially wetting liquids, it has been observed in slowly moving wetting films driven by thermal gradients,[21] making this boundary condition a realistic choice.

The undisturbed solutions to Eqs. (2) and (3) are well described by a traveling wave moving at constant speed c.

Downloaded 28 Oct 2008 to 131.215.237.157. Redistribution subject to AIP license or copyright; see http://pof.aip.org/pof/copyright.jsp

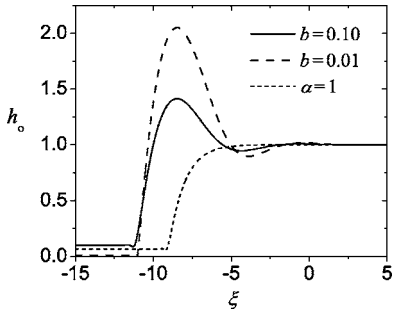

FIG. 3. Numerical solution of the dimensionless, steady state profile, $h_o(\xi)$. Films driven strictly by Marangoni stresses with precursor film thicknesses $b=0.10$ and $b=0.01$ develop pronounced capillary ridges. The film subject to gravitational drainage with $\alpha=1$ and $b=0.065$ has a monotonically decreasing front.

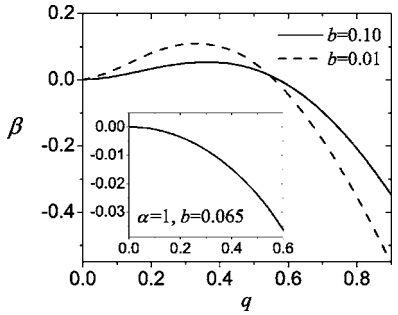

FIG. 4. Dispersion curves, $\beta(q)$, from eigenvalue analysis corresponding to base state profiles shown in Fig. 3. Thinner film exhibits unstable flow for $q \lesssim 0.55$. The inset contains results for the thicker film (without a capillary ridge), which exhibits stable flow for all disturbance wave numbers $q>0$.

These undisturbed solutions are therefore stationary with respect to the coordinate $\xi \equiv \chi + ct$. The equations governing the base state profiles, $h_0(\xi)$, are then given by

$$c_M h_{0\xi} - (h_0^2)_\xi + (h_0^3 h_{0\xi\xi\xi})_\xi = 0 \tag{4}$$

when $h_c \ll \tau/\rho g$, and

$$c_D h_{0\xi} - \frac{3}{3-2\alpha}(h_0^2)_\xi + \frac{2\alpha}{3-2\alpha}(h_0^3)_\xi + (h_0^3 h_{0\xi\xi\xi})_\xi = 0 \tag{5}$$

when $h_c = \alpha\tau/\rho g$. Equations (4) and (5) are first integrated subject to the boundary conditions that $h_0(\xi \to \infty)=1$ and $h_0(\xi \to -\infty)=b$. These conditions determine the overall constant of integration as well as the speed of the traveling wave, which is found to be $c_M = 1+b$ for $h_c \ll \tau/\rho g$ and $c_D = [3(1+b)-2\alpha(1+b+b^2)]/(3-2\alpha)$ for $h_c = \alpha\tau/\rho g$. The remaining third order differential equations are converted to three first order equations that are then solved as an initial value problem.[6,7,56,57,59] Comparison with experiment[6,7] has shown that both the predicted rates of spreading and the profile shapes described by Eqs. (4) and (5) are in very good agreement with observed results.

Typical solutions for the shape of the spreading film near the advancing front with and without gravitational drainage are shown in Fig. 3. The solutions correspond to parameter values $b=0.1$ and $b=0.01$ for $h_c \ll \tau/\rho g$, and $b=0.065$ for $\alpha=1$. The numerical solution to Eqs. (4) and (5) requires input values for b or α, which then uniquely determine the speed and shape of the spreading film. When drainage effects are negligible, the spreading film develops a strong capillary rim at the leading edge, and larger values of b produce smaller ridge amplitudes. When drainage is significant, the flux balance can be accommodated by a film shape with a monotonically decreasing profile and no evidence of a ridge. In this case, once α is specified, there exists only one value of b for which the flux balance is achieved ($\alpha=1$ and $b=0.065$ in Fig. 3). There are no traveling wave solutions for other b corresponding to $\alpha=1$, as other values of b result in continuously evolving profiles or double shock structures, in agreement with the results of Ref. 12. In all calculations the chosen values for b correspond to realistic precursor film thicknesses, and the calculated film profiles agree well with experimental data.[6,7] Experiments reported in the literature for thermally driven films have produced characteristic film thicknesses, h_c, on the order of a micrometer. The value $b=0.1$ therefore corresponds to a prewetting film whose thickness is approximately 1000 Å, which is consistent with a film grown by surface diffusion or van der Waals forces. Results are also presented for $b=0.01$ for comparison.

B. Disturbance analysis of steady state solutions

To capture solutions describing incipient sinusoidal growth of the spreading front in the transverse direction, $\hat{\zeta}$, Eqs. (2) and (3) are perturbed about the steady traveling wave solutions by seeking two-dimensional disturbances of the form

$$h_1(\xi,\zeta,t) = G(\xi,t)\exp(iq\zeta), \tag{6}$$

where q is the dimensionless wave number. Upon linearizing, the governing disturbance equations in the streamwise direction are given by

$$\frac{\partial G}{\partial t} + (1+b)G_\xi - \frac{\partial}{\partial \xi}[2h_0 G - 3h_0^2 h_{0\xi\xi\xi} G - h_0^3(G_{\xi\xi\xi} - q^2 G_\xi)] + h_0^3(q^4 G - q^2 G_{\xi\xi}) = 0 \tag{7}$$

for thin films such that $h_c \ll \tau/\rho g$, and

$$\frac{\partial G}{\partial t} + \frac{3(1+b)-2\alpha(1+b+b^2)}{(3-2\alpha)}G_\xi - \frac{\partial}{\partial \xi}\left[\frac{6}{3-2\alpha}h_0 G - \frac{6\alpha}{3-2\alpha}h_0^2 G - 3h_0^2 h_{0\xi\xi\xi} G - h_0^3(G_{\xi\xi\xi} - q^2 G_\xi)\right] + h_0^3(q^4 G - q^2 G_{\xi\xi}) = 0 \tag{8}$$

for thicker films scaled according to $h_c = \alpha\tau/\rho g$. Both of these equations are subject to the decay conditions $G, G_\xi \to 0$ as $\xi \to \pm\infty$.

1. Modal analysis

Exponential solutions to Eqs. (7) and (8) are sought such that $G(\xi,t) = H(\xi)\exp(\beta t)$, where β denotes the dimensionless disturbance growth rate. The dispersion curves corresponding to the base state profiles shown in Fig. 3 are plotted in Fig. 4. As illustrated by the curves in the larger plot in Fig. 4, there exists a band of wave numbers $0 < q \lesssim 0.55$ for

Downloaded 28 Oct 2008 to 131.215.237.157. Redistribution subject to AIP license or copyright; see http://pof.aip.org/pof/copyright.jsp

which the flow is unstable with a maximum growth rate occurring at $q \approx 0.35$ (and nearly insensitive to the precursor film thickness) when gravitational drainage is negligible. If gravitational drainage provides a counterflow large enough to eliminate the capillary rim at the advancing front, the film is stable to transverse sinusoidal disturbances of all wave numbers, as shown in the inset of Fig. 4. Previous work exploring a larger range of input parameter values has confirmed this observation wherein depletion of the capillary rim enhances film stability,[6,7] as is also the case for a falling film with a significant hydrostatic pressure component normal to the substrate.[35] The shape of the eigensolutions, $H(\xi)$, is shown in Sec. III B.

2. Transient, nonmodal analysis

Equations (7) and (8), which describe the evolution of an infinitesimal disturbance to a thermally driven film, can be expressed in operator form as a linear autonomous matrix $\mathbf{A}$ acting on the discretized disturbance $\boldsymbol{G}$ according to $d\boldsymbol{G}/dt = \mathbf{A}(h_0(\xi);q)\boldsymbol{G}$. The entries of $\mathbf{A}$ consist of the elements obtained from a central difference discretization of Eqs. (7) or (8). Because $\mathbf{A}$ is autonomous (since the base flow is steady in the traveling reference frame), the solution for $\boldsymbol{G}$ is explicitly given by $\boldsymbol{G} = \exp(\mathbf{A}t)\boldsymbol{G}_0$, where $\boldsymbol{G}_0 \equiv \boldsymbol{G}(t=0)$ is the initial disturbance to the film. Because $\mathbf{A}$ is non-normal, the leading eigenvalue β formally determines only the asymptotic stability of the linearized system as $t \to \infty$.[8–10,41] The maximum amplification[9,41] of any disturbance applied to the system at $t=0$ is $\sigma_{\max}(t) = \|\exp(\mathbf{A}t)\|$, which in principle may assume values several orders of magnitude larger than $\exp(\beta t)$. As $t \to \infty$, the growth rate asymptotes to the modal result.

III. RESULTS OF NONMODAL ANALYSIS

The non-normality of $\mathbf{A}$ is due to the spatial inhomogeneity of the base state, $h_0(\xi)$, because terms of the form $h_0^m \partial^n / \partial \xi^n$, where m and n are integers, do not commute with their transpose. The temporal evolution of $\|\exp(\mathbf{A}t)\|$ is examined below in the 2-norm to determine the transient behavior of thermocapillary spreading with a precursor film model. Emphasis is also focused on the propagation of an initial disturbance to its final form at time t through $\exp(\mathbf{A}t)$. The optimal (i.e., most destabilizing) disturbance to the spreading film at $t=0$ and its final state at time t are determined within the linearized theory from the singular value decomposition (SVD) of the propagator[9,41] according to $\exp(\mathbf{A}t) = \mathbf{U}\mathbf{\Sigma}\mathbf{V}^{\dagger}$. The optimal initial disturbance, $\boldsymbol{V}_{\text{opt}}$, is the first column of the unitary matrix $\mathbf{V}$. The corresponding evolved state, $\boldsymbol{U}_{\text{opt}}$, is the first column of the unitary matrix $\mathbf{U}$. The elements of the diagonal matrix $\mathbf{\Sigma}$ determine the amplification of each orthonormal column of $\mathbf{V}$ over the time interval t. The leading entry of $\mathbf{\Sigma}$ then determines the amplification of the optimal disturbance: $\sigma_{\max} = \|\exp(\mathbf{A}t)\|$.

A. Amplification ratio

Matrix norms and singular value decompositions were calculated using MATLAB 5.3.[60] The elements of the matrix $\mathbf{A}$ were obtained from discretization by central differences, and the number of grid points ranged from 1000 to 5000. Care was taken that the computational domain was sufficiently large, as smaller domains would artificially pin the initial disturbances to the far edge of the domain in the precursor film region (equivalent to specifying a maximum spatial extent of the initial disturbance to the precursor film). In order to determine the size of the appropriate domain, the base flow profiles were extended on either side [since $h_0(\xi \to \infty) = 1$ and $h_0(\xi \to -\infty) = b$] and the singular value decomposition computed. The chosen domain size ensured that the value of $\|\exp(\mathbf{A}t)\|$ did not differ and that neither $\boldsymbol{V}_{\text{opt}}$ nor $\boldsymbol{U}_{\text{opt}}$ changed form or location upon reduction.

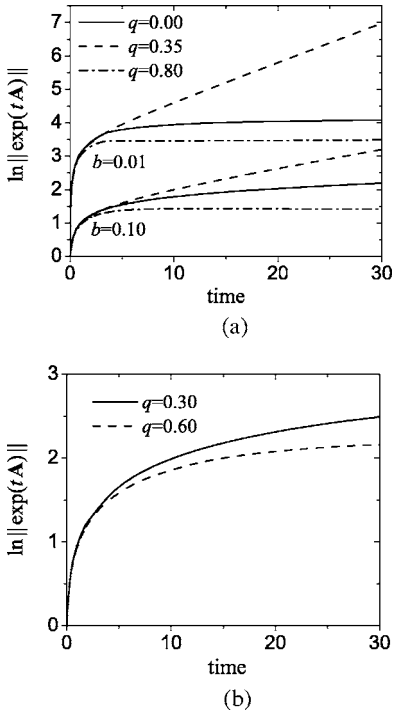

FIG. 5. Maximum possible amplification of disturbances within a time interval t. (a) Thin film driven strictly by thermocapillary stresses for $b=0.10$ and $b=0.01$. (b) Thicker film subject to gravitational drainage where $\alpha=1.0$ and $b=0.065$.

Since all the experiments in the literature have reported rivulet formation within dimensionless times ranging from $1 < t < 15$ (see Sec. IV below) for unstable flows, computations were extended through $t=30$ to ensure that the relevant dynamics were captured. For the cases studied, it was found that by $t=30$, the optimal disturbance had evolved to a shape closely or exactly matching the shape of the eigenfunction predicted from linear stability analysis, indicating that $t=30$ represents reasonably "late" times in the spreading dynamics. Plotted in Fig. 5 is $\ln\|\exp(\mathbf{A}t)\|$ for several wave numbers q corresponding to the base states shown in Fig. 3. Results for a thin film, $h_c \ll \tau/\rho g$, are plotted in the top figure, while the bottom figure contains plots for a thicker film with $h_c = \tau/\rho g$.

There is a modest amount of nonmodal amplification of disturbances, as indicated primarily by the nonlinear portions of the curves at early times in Fig. 5(a). This growth arises from the interaction of the nonorthogonal eigenvectors with different decay rates. The transient amplification depends rather strongly on the precursor film thickness[35,36] b (in-

Downloaded 28 Oct 2008 to 131.215.237.157. Redistribution subject to AIP license or copyright; see http://pof.aip.org/pof/copyright.jsp

creases with decreasing b) but only weakly on the wave number q. Exponential growth corresponding to the largest eigenvalue found from modal analysis begins around $t=10$ shear times for the $q=0.35$ mode, which indicates that the system relatively quickly converges to the unstable state predicted by modal linear stability theory. Disturbances with asymptotically stable wave numbers begin to decay exponentially by the time at which the contact line has spread over the length of the precursor film used for the computations. The domain size in these computations was sufficiently long that this decay is not evident at the times shown in the figures. Transient amplification is sustained while disturbances to the precursor film are convected to the contact line in the moving reference frame, as explained in Sec. IV below. Disturbances to the macroscopic capillary ridge do not undergo significant transient growth.

The curves in Fig. 5(b) represent the growth of disturbances applied to the base state shown in Fig. 3 with significant drainage. The response to disturbances of wave number $q=0.30$ and $q=0.60$ mimic the ordering in the decay rate predicted in Fig. 4. This system experiences modest transient growth that slowly decays to an asymptotically stable state. Because the corresponding values of $\beta(q)$ in Fig. 4 are of order 10^{-2}, the decay is rather gradual and is not visible in Fig. 5(b). The extremely long domains required to capture the decay of disturbances of arbitrary spatial extent at the correspondingly large times require excessive computational time. As discussed below in Sec. IV, perturbations encountered in experiments should have a finite spatial extent, and the decay of such disturbances will be much more rapid. The amplification ratios plotted in Fig. 5 represent the maximum possible amplification of arbitrary disturbances. For given experimental conditions, the amplification should be less because the perturbations will be of finite extent and may not be of optimal form.

B. Optimal perturbations

It is also of interest to investigate the particular disturbances that elicit maximal response during the spreading process and to relate these functions to the shape and location of the eigenfunctions obtained from modal linear stability theory. These results elucidate the most vulnerable regions of the film to perturbations. Shown in Figs. 6–8 are the optimal initial states, $\boldsymbol{V}_{\mathrm{opt}}$, and corresponding final states, $\sigma_{\max}\boldsymbol{U}_{\mathrm{opt}}$, obtained from SVD decomposition of the propagator, $\exp(\mathbf{A}t)$. Figures 6 and 7 show plots of excitations for two selected wave numbers, $q=0.35$ and $q=0.80$, which are representative of asymptotically unstable and stable states, respectively, when gravitational drainage is negligible. Figure 8 shows plots of excitations for wave number $q=0.60$ applied to a film stabilized by gravitational drainage. The magnitude of the optimal disturbances, $\boldsymbol{V}_{\mathrm{opt}}(t)$, is normalized to unity, and the magnitude of the evolved states correspond to the amplification of $\boldsymbol{V}_{\mathrm{opt}}(t)$ over the time t (as shown in Fig. 5) so that the evolution of the different perturbations can be compared.

Figure 6 contains plots of the optimal initial excitations and corresponding responses for an asymptotically unstable wave number, $q=0.35$. The disturbance applied at $t=0$ that elicits the largest response at $t=1$ is centered in the precursor region just forward of the apparent contact line near the forward part of the capillary ridge, which supports the interpre-

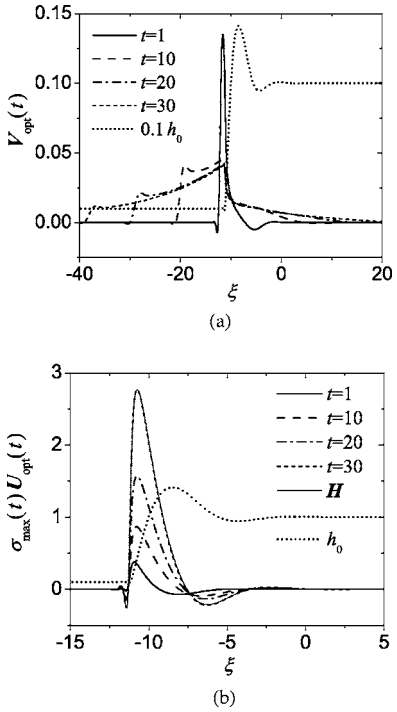

FIG. 6. (a) Normalized optimal initial excitation, $\boldsymbol{V}_{\mathrm{opt}}$, and (b) the evolved state after time t, $\sigma_{\max}\boldsymbol{U}_{\mathrm{opt}}$, for a disturbance of wave number, $q=0.35$, applied to the base state with $b=0.1$ shown in Fig. 3. The eigenfunction H found from linear stability theory is plotted alongside the curves in (b).

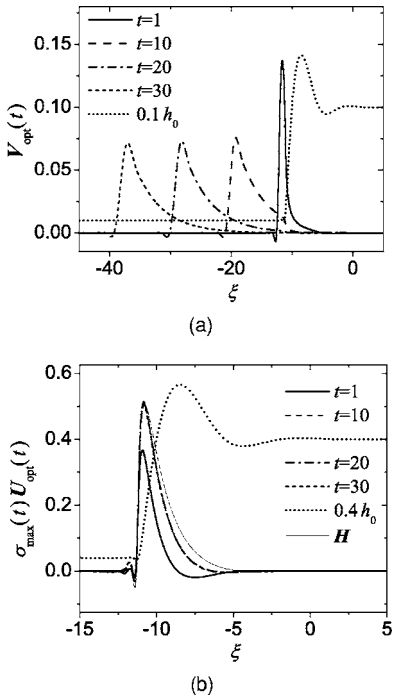

FIG. 7. (a) Normalized optimal initial excitation, $\boldsymbol{V}_{\mathrm{opt}}$, and (b) the evolved state after time t, $\sigma_{\max}\boldsymbol{U}_{\mathrm{opt}}$, for a disturbance of wave number, $q=0.80$, applied to the base state with $b=0.1$ shown in Fig. 3. The eigenfunction H found from linear stability theory is plotted alongside the curves in (b).

Downloaded 28 Oct 2008 to 131.215.237.157. Redistribution subject to AIP license or copyright; see http://pof.aip.org/pof/copyright.jsp

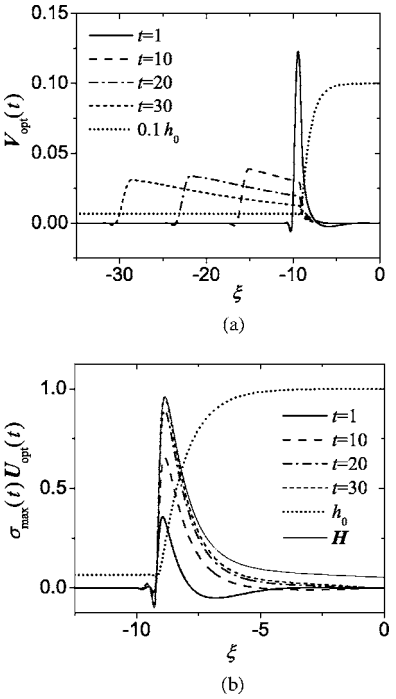

FIG. 8. (a) Normalized optimal initial excitation, $\boldsymbol{V}_{\text{opt}}$, and (b) the evolved state after time t, $\sigma_{\max}\boldsymbol{U}_{\text{opt}}$, for a disturbance of wave number, $q=0.60$, applied to the base state with $\alpha=1$ and $b=0.065$ shown in Fig. 3. The eigenfunction H found from linear stability theory is plotted alongside the curves in (b).

tation of the contact line as a noise amplifier.[35,36] The corresponding evolved state is focused at the nominal contact line and forward portion of the capillary ridge. The initial disturbances that elicit the maximal response at later times extend further ahead of the contact line into the precursor region and also broaden to encompass much of the capillary ridge while maintaining a peak of maximum amplitude at the contact line, which is the most vulnerable region of the film. By a dimensionless time $t=30$ the evolved state is nearly indistinguishable from the eigenfunction calculated from the standard modal theory, and the optimal disturbance is quantitatively similar to the corresponding eigenfunction of the adjoint linear operator. Evolved states corresponding to the optimal disturbances from earlier times asymptote to the leading eigenfunction even more quickly, as the transient period is shorter for disturbances of smaller spatial extent.

The initial excitations and evolved responses for an asymptotically stable wave number, $q=0.80$, are plotted in Fig. 7. The optimal initial excitations for short times are localized near the apparent contact line, as they are for unstable wave numbers. The excitations that induce the optimal response at later times, however, do not broaden to encompass any of the capillary ridge but migrate further into the precursor film. The differences between Figs. 6 and 7 indicate that while the initial perturbations that induce the optimal response at later times for unstable wave numbers encompass most of the spreading film, the analogous excitations for stable wave numbers are confined to a region beyond the nominal contact line.

By contrast, Fig. 8 contains plots of the response for a thicker film in which gravitational drainage has eliminated the presence of the capillary ridge. While the film is asymptotically stable, the optimal initial disturbances differ from Fig. 7 in that they quickly broaden to encompass the spreading film and the entire precursor region. The majority of the initial disturbance is weighted toward the precursor film as before but still includes the nominal contact line. The responses asymptote toward the eigenfunction, $H(\xi)$, more slowly than in Fig. 7 because the associated growth rates, $\beta(q)$, are smaller by an order of magnitude.

A straightforward physical interpretation can be given to the optimal initial disturbance, $\boldsymbol{V}_{\text{opt}}$, that is applied to the system at time $t=0$. The system's response, given by the corresponding final state, $\sigma_{\max}\boldsymbol{U}_{\text{opt}}$, is the evolved disturbance after the specified time interval t. A disturbance applied to the precursor film elicits a significant response from the system once the apparent contact line at the front of the capillary ridge encounters the disturbance. A disturbance applied far ahead of the capillary ridge will not induce a significant response until the film has spread far enough to encounter the disturbance. The base states are computed in a moving reference frame in which the initial disturbances are convected toward the stationary film. Disturbances that elicit the maximum response at short times are therefore focused at the apparent contact line, while the optimal initial disturbances at later times migrate further into the precursor region so that they will continually excite the system over several units of dimensionless time. In the limit $t\to\infty$ the most unstable mode, $H(\xi)$, dominates the system's response to perturbations. Since the linearized disturbance operator is nonnormal, this mode is optimally excited by its associated adjoint eigenvector, H^* $[\lim_{t\to\infty}\boldsymbol{V}_{\text{opt}}(t)=\boldsymbol{H}^*]$.[41] If the linearized disturbance operator were normal, then the optimal disturbance would be the leading eigenvector and would not extend into the precursor film, as H and H^* differ significantly in shape.

For asymptotically stable wave numbers, the peaks of maximal amplitude for later times migrate far into the precursor film. Because the system is asymptotically stable to these perturbations, the optimal response is obtained if the contact line encounters the perturbation close to the time at which the maximum is being sought. The optimal perturbations shown in Fig. 7(a) for each time t would be convected (in the moving frame) to the front of the capillary ridge just prior to the time being considered. If the contact line and front of the capillary ridge were perturbed only at time $t=0$, the response would have decayed away by time $t\gg 1$.

For the slip model of the contact line,[9,10] by contrast, the optimal disturbances of any wave number exhibit a peak of maximum amplitude at the contact line, and disturbances to the macroscopic film quickly undergo behavior predicted by modal analysis with little transient growth. The structure of optimal excitations for the slip[10] and precursor film models are compared in Fig. 9 for the wave number $q=0.35$. At $t=1$, the optimal excitations for each model have a peak of maximal amplitude centered at the contact line at $\xi=0$. By $t=10$, however, the excitations for the precursor film model extend well into the precursor film ahead of the nominal contact line. This shape allows a much longer excitation of

Downloaded 28 Oct 2008 to 131.215.237.157. Redistribution subject to AIP license or copyright; see http://pof.aip.org/pof/copyright.jsp

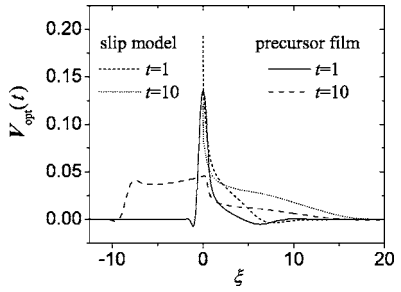

FIG. 9. Comparison of the optimal excitations, $\boldsymbol{V}_{\mathrm{opt}}(t)$, from the slip and precursor film models for the unstable wavenumber $q=0.35$ at times $t=1$ and $t=10$. The parameters are $b=0.1$ and $\alpha=0$ for the precursor film model. The calculations for the slip model (Ref. 10) use a slip coefficient of 0.1 and a contact slope of 0.1.

the nominal contact line as the film spreads over the perturbations, leading to larger transient growth. These results further demonstrate that most of the nonmodal growth occurs as the contact line of the spreading film adjusts to perturbations. Because disturbances to the film cannot extend beyond the contact line for the slip model, and because the contact slope is fixed in most applications of that model, the amount and duration of the nonmodal amplification are significantly less than for the precursor film model considered here. These restrictions on the slip model can be at least partially overcome by allowing disturbances to the slip coefficient[61] and by formulating the problem in terms of a speed-dependent contact angle[62] that can adjust to perturbations.

There are meaningful differences between perturbations to the precursor film and slip coefficient due to the wetting properties of the liquid, however. Perturbations to the precursor film of a wetting fluid can correspond to actual perturbations in the film thickness because the liquid wets the substrate ahead of the nominal contact line. For partially wetting fluids described by the slip model, however, perturbations to the film cannot extend beyond the actual contact line. Perturbations of the slip coefficient can be used to represent surface heterogeneity that the film encounters as it spreads, and the resulting transient behavior would correspond the response of the film to external (parametric) forcing. A more detailed comparison of the transient behavior of disturbances to thermally driven films with different contact line models can be found in Ref. 63. A recent comparison of transient growth in films driven by gravity for slip and precursor film models is given in Ref. 46.

IV. DISCUSSION

While the finite time behavior of disturbances governed by non-normal operators can only be formally described by a transient analysis, the quantification of "early" or "late" times depends critically on the characteristic shear time of a particular flow configuration and the time of experimental observation. For unstable flow, the relevant ratio is the onset time for instability versus the characteristic shear time. Previous detailed comparison of all available experimental data with the results of eigenvalue analysis for the thermally driven film has proved quite favorable. Recent studies employing slip[9,10] and a structured (van der Waals) precursor film[8] to model the contact line demonstrated that for these models the transient growth is small and of short duration, which explained the accuracy of modal analysis of the non-normal system. The flat precursor film model considered here admits more sustained transient growth than do the other two models, although the asymptotic predictions are identical.[10,63] Careful analysis reveals that the characteristics of this transient growth and the optimal disturbances are consistent with these other studies and their strong agreement with experimental results due to the moderate amount of possible transient growth and the rapid approach to the solutions from modal theory.

Although several independent groups have conducted experiments on thermally driven films with and without drainage effects, the onset time for corrugation and fingering at the advancing front has only explicitly been measured in a few cases. A review of the available literature reveals five representative experiments for which some data exists on the timescale of observation and the onset time for instability. An extensive comparison between experiment and predictions from modal linear stability theory for the shape and speed of the base flow profiles, the wavelength selected by experiment, and the finger growth rate within the linear regime yielded excellent agreement.[6,7] Table I contains the parameter values and estimates of the characteristic shear time, t_s, for each experiment along with the estimated time, t_o, at which the front corrugation first appears (for unstable flow),

TABLE I. Parameter values used to estimate the characteristic shear time, t_s, and the observation time, t_o, for fingering onset or stable flow. The last column represents the number of shear times that have elapsed by finger onset (in unstable flows) or during the observation period (for stable flows). Remaining variables are described in the text.

Reference	η (ps)	τ (dyn/cm^2)	Stable (S) or Unstable (U)	l (μm)	U_{exp} (μm/s)	$t_s=l/U_{\mathrm{exp}}$ (s)	t_o (s)	$t=t_o/t_s$
6	0.20	2.1	U	25	3	8.3	90	11
6 and 9	0.20	1.0	U	20	1	20	<300	<15
10	0.48	0.35	U	467	5.76	81	60	1.4
5	0.31	0.086	S	168	0.053	3170	$\leq$24 h	≤27
5	0.27	0.185	S	263	0.249	1056	$\leq$24 h	≤82

Downloaded 28 Oct 2008 to 131.215.237.157. Redistribution subject to AIP license or copyright; see http://pof.aip.org/pof/copyright.jsp

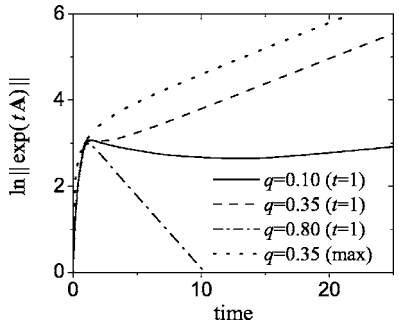

FIG. 10. Amplification of $\boldsymbol{V}_{\mathrm{opt}}(t=1)$ vs t for a thin film and $b=0.01$. The transient amplification ceases as soon as the contact line passes over the disturbance. Similar curves result from using a short length of precursor film to compute $\ln\|\exp(\mathbf{A}t)\|$, which is equivalent to limiting the maximum extent of the initial disturbance.

or the maximum observation time (for stable flow). The onset of unstable flow is taken to be the point in time at which the spreading front is first observed to undergo a coherent transverse corrugation (that later develops into liquid rivulets). The unstable films were observed to undergo spanwise corrugation within a time interval $1<t<15$, depending on experimental conditions. For stable flow, no frontal corrugation was observed even after 30–80 shear times (the duration of the experiments). The time scales relevant to unstable flow are therefore contained within the time intervals studied in Figs. 5–8. More significantly, as suggested by Figs. 5 and 6, the exponential regime establishes itself well within ten shear times for the most asymptotically unstable wave numbers observed in experiments, which likely explains the success of eigenvalue analysis in predicting the various characteristics of thermally driven films. The transient period thus corresponds to short experimental times (on the order of several minutes or less), and the system quickly undergoes a fingering instability whose features are very well predicted by modal linear stability theory.

The rapid onset of the exponential regime for short disturbances (characteristic of experimental noise) is clearly evident in Fig. 10, which contains a plot of the amplification from the propagation of $\boldsymbol{V}_{\mathrm{opt}}(t=1)$ forward in time for a thin film in which drainage is negligible. The transient growth ceases as soon the contact line passes over the disturbance, which occurs just after $t=1$, and demonstrates that the "long-time" modal regime may be attained very early in the spreading dynamics. A similarly rapid transition to modal growth occurs as soon as the contact line passes over longer disturbances. Long disturbances to the precursor film are analogous to exciting the contact line region of the film continuously (as the disturbances are convected toward it), and disturbances of such long extent, which are the optimal disturbances for larger times, are unlikely to occur in experiments on smooth and homogeneous substrates. Even for these optimal disturbances of arbitrarily long extent, however, the modal regime is approached by $t\approx 10$ shear times for $q=0.35$, the most asymptotically unstable wave number.

There are two scenarios in which transient growth could invalidate the results from a modal linear stability analysis.[14] In a purely linear scenario,[35] an initial disturbance with wave number q and magnitude $\|\boldsymbol{G}_0\|=a$ could be transiently amplified by the factor d, thereby producing a perturbation of magnitude $ad=\mathcal{O}(1)$. The transient effects would dominate if $d \gtrsim a^{-1}$ and if this amplification were to occur on a time scale shorter than $1/\beta(q_{\max})$, which would result in fingers with wave number q rather than $q_{\max}$. In a second scenario,[14,37] an initial disturbance could be transiently amplified by the linear part of the evolution operator, and the nonlinear terms could produce secondary disturbances that are further transiently amplified. This mechanism could lead to a positive feedback loop and nonlinear "bootstrapping," although this type of nonlinear instability seems unlikely for typical experimental conditions. Physically, transient growth occurs as disturbances to the precursor film interact with the nominal contact line, and the amplified structure (the evolved state at time t) is located at the forward portion of the capillary ridge or monotonic front (see Figs. 6–8). Secondary disturbances produced by the nonlinear terms are not expected to propagate ahead of the spreading film and to reexcite the contact line (as disturbances are convected from the precursor film to the contact line in the moving reference frame), which is required for further amplification.

While transient growth may not be important for thin films with capillary ridges because of the rapid attainment of modal growth, it may be more significant for thicker films without capillary ridges. Because the leading eigenvalues for the monotonic front shown in Fig. 8 are small in magnitude and negative, there is a slow decay to the modal results (longer period of transient growth), as shown in Fig. 5(b). For this case, initial perturbations of magnitude close to the precursor film thickness (b) can be amplified by a factor $\approx b^{-1}$, which in theory may make possible the purely linear scenario for transient effects to be important. Since instability is not observed in experiments, however, transient effects must not be physically significant. The predicted transient linear dynamics based on the precursor film model must therefore be interpreted carefully. These conclusions are in agreement with recent nonlinear computations[16] that show the strong stability of the advancing front of double shock structures that can occur in thermally driven climbing films.

There are several possible reasons for which the predictions of modal theory agree with experiment despite the presence of transient growth. Very long optimal disturbances (or long precursor films) may not be physically realized in experiments on homogeneous surfaces, the disturbances arising from experimental "noise" may be much smaller than the thickness of the precursor film appropriate for theoretical studies, or the precursor film model may not adequately capture the transient dynamics of spreading films. Alternatively, while disturbances that can undergo significant transient growth might be realized under experimental conditions, nonlinear effects could suppress the disturbance amplification in linearly stable films. Such strong nonlinear suppression of disturbances was reported for the case of a falling film along an inclined plane.[64] These results are expected to hold for thermally driven films because of the similarities of the governing equations, and a weakly nonlinear analysis and fully nonlinear simulations of the evolution of disturbances to the film could verify these effects for the thermocapillary

Downloaded 28 Oct 2008 to 131.215.237.157. Redistribution subject to AIP license or copyright; see http://pof.aip.org/pof/copyright.jsp

spreading considered here. Similar computational studies employing a transversely modulated precursor film to mimic patterned surfaces have been used to assess the nonlinear dynamics and interactions of perturbations of different wave numbers for films spreading along inclined planes.[47–52] Experiments on spreading films on chemically patterned surfaces[65] could also be used to assess the predictions of transient dynamics, as the patterning could impose small but long disturbances of specified wave number. Determining the response to these perturbations and the size of the perturbations required to induce instability in linearly stable films (if possible) would provide useful comparisons for further theoretical work.

V. CONCLUSION

The transient behavior and stability characteristics of a climbing film driven to spread by a constant shear stress applied via a linear temperature profile have been examined for a flat precursor film model. The maximum amplification of disturbances applied to thin films driven strictly by Marangoni stresses and to thicker films whose flow is modulated by the additional presence of gravitational drainage has been studied. The steady state film profiles for these two examples differ considerably. In particular, the thinner films develop a pronounced capillary ridge at the leading edge that is quite susceptible to lateral breakup and rivulet formation, while the thicker films do not develop a ridge and are asymptotically stable. Because the linearized disturbance operator, $\mathbf{A}$, for these systems is non-normal, a transient analysis was used to determine the maximum amplification of arbitrary initial disturbances and the optimal (most destabilizing) excitations to the spreading film. Comparison with experiment reveals that the transient period is relatively short lived and terminates as soon as the contact line passes over the perturbation, which likely explains the success of the long-time analysis in describing various details of the spreading film and fingering behavior.

For both asymptotically stable and unstable flows, the optimal excitations initially are narrowly focused at the nominal contact line. As time increases these disturbances broaden significantly and extend far into the precursor region ahead of the spreading film. Optimal disturbances corresponding to asymptotically unstable flows also encompass the entire thick portion of the film. The shape of the optimal disturbances and adjoint eigenvectors confirms that the contact line is the region of the film most vulnerable to perturbations. For thin films that are asymptotically unstable, modal growth corresponding to the most unstable eigenvalue is recovered early in the spreading dynamics, which explains the accuracy of modal linear stability predictions in describing various characteristics of the fingering instability observed in experiments. For thicker films that are asymptotically stable, the transient regime can persist much longer. Experiments for this regime have confirmed the linear stability predictions, indicating that transient growth does not induce instability. Taken together, studies of the optimal excitations in thermocapillary spreading for different contact line models[8–10,63,66] therefore reveal that disturbances extending far ahead of the contact line most effectively destabilize the spreading film. Such disturbances to the film thickness can occur in the wetting films appropriately described by the precursor film model, in which the fluid wets the substrate ahead of the nominal contact line. For the partially wetting films described by a slip model, however, such disturbances to the film thickness cannot occur, and the transient amplification is less (although the modal results agree quantitatively). Additional insight into the transient dynamics of these systems may be gained from further analysis of the nonlinear evolution of disturbances and experiments on micropatterned surfaces, which could provide a controlled method of introducing surface heterogeneity.

ACKNOWLEDGMENTS

This work was partially supported by the National Science Foundation (CTS and ECS programs) and the NASA Microgravity Fluid Physics Program. S.M.T. also gratefully acknowledges the financial support of the Moore Distinguished Scholar Program at the California Institute of Technology.

[1] C. H. Ho and Y. C. Tai, "Micro-electro-mechanical-systems (MEMS) and fluid flows," Annu. Rev. Fluid Mech. **30**, 579 (1998).
[2] M. Gad-El-Hak, "The fluid mechanics of microdevices—The Freeman Scholar lecture," J. Fluids Eng. **121**, 5 (1999).
[3] A. A. Darhuber, J. M. Davis, S. M. Troian, and W. W. Reisner, "Thermocapillary actuation of liquid flow on chemically patterned surfaces," Phys. Fluids **15**, 1295 (2003).
[4] A. A. Darhuber and S. M. Troian, "Principles of microfluidic actuation by modulation of surface stresses," Annu. Rev. Fluid Mech. **37**, 425 (2005).
[5] D. E. Kataoka and S. M. Troian, in *Dynamics in Small Confining Systems III*, edited by J. M. Drake, J. Klafter, and R. Kopelman (Materials Research Society, Pittsburgh, PA, 1997).
[6] D. E. Kataoka and S. M. Troian, "A theoretical study of instabilities at the advancing front of thermally driven coating films," J. Colloid Interface Sci. **192**, 350 (1997).
[7] D. E. Kataoka and S. M. Troian, "Stabilizing the advancing front of thermally driven coating films," J. Colloid Interface Sci. **203**, 335 (1998).
[8] J. M. Davis and S. M. Troian, "Influence of attractive van der Waals interactions on the optimal excitations in thermocapillary driven spreading," Phys. Rev. E **67**, 016308 (2003).
[9] J. M. Davis, B. J. Fischer, and S. M. Troian, in *Interfacial Fluid Dynamics and Transport Processes, Lecture Notes in Physics*, edited by R. Narayanan (Springer, Heidelberg, 2003), pp. 79–106.
[10] J. M. Davis and S. M. Troian, "Influence of boundary slip on the optimal excitations in thermocapillary driven spreading," Phys. Rev. E **70**, 046309 (2004).
[11] A. L. Bertozzi, A. Munch, X. Fanton, and A. M. Cazabat, "Contact line stability and 'undercompressive shocks' in driven thin film flows," Phys. Rev. Lett. **81**, 5169 (1998).
[12] A. L. Bertozzi, A. Munch, and M. Shearer, "Undercompressive shocks in thin film flows," Physica D **134**, 431 (1999).
[13] A. A. Golovin, B. Y. Rubinstein, and L. M. Pismen, "Effect of van der Waals interactions on the fingering instability of thermally driven thin wetting films," Langmuir **17**, 3930 (2001).
[14] R. O. Grigoriev, "Contact line instability and pattern selection in thermally driven liquid films," Phys. Fluids **15**, 1363 (2003).
[15] R. Buckingham, M. Shearer, and A. Bertozzi, "Thin film traveling waves and the Navier slip condition," SIAM J. Appl. Math. **63**, 722 (2003).
[16] M. Bowen, J. Sur, A. L. Bertozzi, and R. P. Behringer, "Nonlinear dynamics of two-dimensional undercompressive shocks," Physica D **209**, 36 (2005).
[17] J. Sur, T. P. Witelski, and R. P. Behringer, "Steady-profile fingering flows in Marangoni driven thin films," Phys. Rev. Lett. **93**, 247803 (2004).
[18] J. Sur, A. L. Bertozzi, and R. P. Behringer, "Reverse undercompressive shock structures in driven thin film flow," Phys. Rev. Lett. **90**, 126105 (2003).

Downloaded 28 Oct 2008 to 131.215.237.157. Redistribution subject to AIP license or copyright; see http://pof.aip.org/pof/copyright.jsp

[19] A. L. Bertozzi, A. Munch, M. Shearer, and K. Zumbrun, "Stability of compressive and undercompressive thin film travelling waves," Eur. J. Appl. Math. **12**, 253 (2001).
[20] A. Munch and A. L. Bertozzi, "Rarefaction-undercompressive fronts in driven films," Phys. Fluids **11**, 2812 (1999).
[21] V. Ludviksson and E. N. Lightfoot, "The dynamics of thin liquid films in the presence of surface-tension gradients," AIChE J. **17**, 1166 (1971).
[22] N. Garnier, R. O. Grigoriev, and M. F. Schatz, "Optical manipulation of microscale fluid flow," Phys. Rev. Lett. **91**, 054501 (2003).
[23] A. M. Cazabat, F. Heslot, S. M. Troian, and P. Carles, "Fingering instability of thin spreading films driven by temperature gradients," Nature (London) **346**, 824 (1990).
[24] A. M. Cazabat, F. Heslot, P. Carles, and S. M. Troian, "Hydrodynamic fingering instability of driven wetting films," Adv. Colloid Interface Sci. **39**, 61 (1992).
[25] P. Carles and A.-M. Cazabat, "The thickness of surface-tension-gradient-driven spreading films," J. Colloid Interface Sci. **157**, 196 (1993).
[26] P. Carles, S. M. Troian, A. M. Cazabat, and F. Heslot, "Hydrodynamic fingering instability of driven wetting films: Hindrance by diffusion," J. Phys.: Condens. Matter **2**, SA477 (1990).
[27] J. B. Brzoska, F. Brochard-Wyart, and F. Rondelez, "Exponential growth of fingering instabilities of spreading films under horizontal thermal gradients," Europhys. Lett. **19**, 2 (1992).
[28] S. M. Troian, E. Herbolzheimer, S. A. Safran, and J. F. Joanny, "Fingering instabilities of driven spreading films," Europhys. Lett. **10**, 25 (1989).
[29] H. E. Huppert, "Flow and instability of a viscous current down a slope," Nature (London) **300**, 427 (1982).
[30] J. M. Jerrett and J. R. deBruyn, "Finger instability of a gravitationally driven contact line," Phys. Fluids A **4**, 234 (1992).
[31] J. R. deBruyn, "Growth of fingers at a driven three-phase contact line," Phys. Rev. A **46**, R4500 (1992).
[32] L. H. Tanner, "Drops," Recherche **174**, 182 (1986).
[33] F. Melo, J. Joanny, and S. Fauve, "Fingering instability of spinning drops," Phys. Rev. Lett. **63**, 1958 (1989).
[34] N. Fraysse and G. M. Homsy, "An experimental study of rivulet instabilities in centrifugal spin coating of viscous Newtonian and non-Newtonian fluids," Phys. Fluids **6**, 1491 (1994).
[35] A. L. Bertozzi and M. P. Brenner, "Linear stability and transient growth in driven contact lines," Phys. Fluids **9**, 530 (1997).
[36] L. Kondic and A. L. Bertozzi, "Nonlinear dynamics and transient growth of driven contact lines," Phys. Fluids **11**, 3560 (1999).
[37] L. N. Trefethen, A. E. Trefethen, S. C. Reddy, and T. A. Driscoll, "Hydrodynamic stability without eigenvalues," Science **261**, 578 (1993).
[38] S. C. Reddy, P. J. Schmid, and D. S. Henningson, "Pseudospectra of the Orr-Sommerfeld operator," SIAM J. Appl. Math. **53**, 15 (1993).
[39] B. F. Farrell, "Optimal excitation of perturbations in viscous shear flow," Phys. Fluids **31**, 2093 (1988).
[40] K. M. Butler and B. F. Farrell, "Three-dimensional optimal perturbations in viscous shear flow," Phys. Fluids A **4**, 1637 (1992).
[41] B. F. Farrell and P. J. Ioannou, "Generalized stability theory. Part 1: Autonomous operators," J. Atmos. Sci. **53**, 2025 (1996).
[42] L. H. Tanner, "The spreading of silicone oil drops on horizontal surfaces," J. Phys. D **12**, 1473 (1979).
[43] P. G. deGennes, "Wetting: Statics and dynamics," Rev. Mod. Phys. **57**, 827 (1985).
[44] J. M. Davis and S. M. Troian, "On a generalized approach to the linear stability of spatially nonuniform thin film flows," Phys. Fluids **15**, 1344 (2003).
[45] V. G. Friz, "Über den dynamischen randwinkel im fall der vollständigen benetzung," Z. Angew. Phys. **19**, 374 (1965).
[46] R. O. Grigoriev, "Transient growth in driven contact lines," Physica D **209**, 105 (2005).
[47] J. A. Diez and L. Kondic, "Contact line instabilities of thin liquid films," Phys. Rev. Lett. **86**, 632 (2001).
[48] L. Kondic and J. A. Diez, "Pattern formation in the flow of thin films down an incline: Constant flux configuration," Phys. Fluids **13**, 3168 (2001).
[49] L. Kondic and J. Diez, "Flow of thin films on patterned surfaces: Controlling the instability," Phys. Rev. E **65**, 045301 (2002).
[50] L. Kondic and J. A. Diez, "Flow of thin films on patterned surfaces," Colloids Surf., A **214**, 1 (2003).
[51] L. Kondic and J. Diez, "Instabilities in the flow of thin films on heterogeneous surfaces," Phys. Fluids **16**, 3341 (2004).
[52] L. Kondic and J. A. Diez, "On nontrivial traveling waves in thin film flows including contact lines," Physica D **209**, 135 (2005).
[53] M. Schneemilch and A. M. Cazabat, "Shock separation in wetting films driven by thermal gradients," Langmuir **16**, 9850 (2000).
[54] A. Oron, S. H. Davis, and S. G. Bankoff, "Long-scale evolution of thin liquid films," Rev. Mod. Phys. **69**, 931 (1997).
[55] X. Fanton, A. M. Cazabat, and D. Quéré, "Thickness and shape of films driven by a Marangoni flow," Langmuir **12**, 5875 (1996).
[56] E. O. Tuck and L. W. Schwartz, "A numerical and asymptotic study of some third-order ordinary differential equations relevant to draining and coating flows," SIAM Rev. **32**, 453 (1990).
[57] G. F. Teletzke, H. T. Davis, and L. E. Scriven, "How liquids spread on solids," Chem. Eng. Commun. **55**, 41 (1987).
[58] M. A. Spaid and G. M. Homsy, "Stability of Newtonian and viscoelastic dynamic contact lines," Phys. Fluids **8**, 460 (1996).
[59] J. A. Moriarty, L. Schwartz, and E. O. Tuck, "Unsteady spreading of thin liquid films with small surface tension," Phys. Fluids A **3**, 733 (1991).
[60] *MATLAB 5.2* (The MathWorks, Natick, MA, 1998).
[61] K.-H. Hoffmann, B. Wagner, and A. Munch, "On the generation and spreading of 'finger' instabilities in film coating processes," in *High Performance Scientific and Engineering Computing*, Vol. 8 of Lecture Notes in Computational Science and Engineering, edited by H.-J. Bungartz, F. Durst, and C. Zenger (Springer, Berlin, 1999), pp. 245–254.
[62] P. G. Lopez, M. J. Miksis, and S. G. Bankoff, "Non-isothermal spreading of a thin liquid film on an inclined plane," J. Fluid Mech. **324**, 261 (1996).
[63] J. M. Davis, "Dynamics and linear stability of thermocapillary spreading films on homogeneous and micropatterned surfaces," Ph.D. thesis, Princeton University, 2003.
[64] Y. Ye and H.-C. Chang, "A spectral theory for fingering on a prewetted plane," Phys. Fluids **11**, 2492 (1999).
[65] D. E. Kataoka and S. M. Troian, "Patterning liquid flow on the microscopic scale," Nature (London) **402**, 764 (1999).
[66] D. Kataoka, "The spreading behavior of thermally driven liquid films," Ph.D. thesis, Princeton University, 1999.

Downloaded 28 Oct 2008 to 131.215.237.157. Redistribution subject to AIP license or copyright; see http://pof.aip.org/pof/copyright.jsp